

Dexamethasone-Loaded Injectable *In-situ* Thermal Crosslinking Magnetic Responsive Hydrogel for the Physicochemical Stimulation of Acupoint to Suppress Pain in Sciatica Rats

Cell Transplantation
Volume 31: 1–14
© The Author(s) 2022
Article reuse guidelines:
sagepub.com/journals-permissions
DOI: 10.1177/09636897221126088
journals.sagepub.com/home/ctj
SAGE

Wan Wei¹, Qihong Yang¹, Jing Hu¹, Yong Yao¹, and Huayuan Yang¹ 

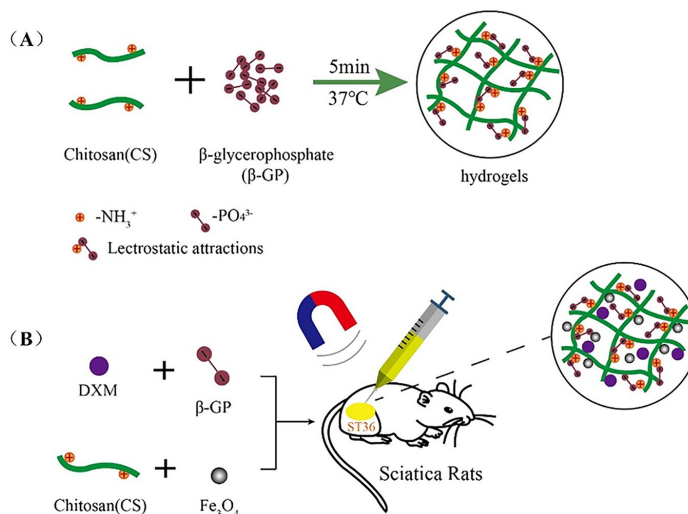
Abstract

The physicochemical stimulation of acupoints is a widespread treatment strategy for different diseases, such as sciatica. Its efficacy is mainly based on the temporal and spatial modulation of the physicochemical properties of the acupoints. The existing therapies based on the stimulation of acupoints have certain disadvantages. Therefore, in this study, injectable dexamethasone (DXM)- and magnetic Fe₃O₄ nanoparticles-loaded chitosan/ β -glycerophosphate (CS/GP) thermal crosslinking hydrogels were prepared, thereby improving the performance of embedding materials. The sciatica rat models were established to compare the therapeutic effects of hydrogels and catgut. The DXM or Fe₃O₄-loaded CS/GP hydrogels were compared in terms of their gelation kinetics, release kinetics, magnetic responsiveness *in-vitro*, and biocompatibility as well as their analgesic effects on the chronic constriction injury of the sciatic nerve (CCI) rats *in-vivo*. The CS/GP/Fe₃O₄/DXM hydrogel showed comparable gelation kinetics and good magnetic responsiveness *in-vitro*. This hydrogel could relieve sciatica by reducing the expression levels of inflammatory factors in serum, inhibiting the p38MAPK (p38, mitogen-activated protein kinase) phosphorylation, and decreasing the expression level of the P2X4 receptor (P2X4R) in the spinal dorsal horn. In conclusion, the DXM or Fe₃O₄-loaded CS/GP hydrogels can be considered as a treatment option for the physicochemical stimulation therapy of acupoints to improve sciatica.

Keywords

injectable hydrogel, magnetic responsiveness, pain-relieving, physicochemical stimulation of acupoint, P2X4R

Graphical abstract



(A) Synthesis route of CS/GP hydrogel **(B)** Fe₃O₄ and DXM encapsulated CS/GP hydrogel used in sciatica rat models under 0.4 T static magnetic field at acupuncture point ST36 (Zusanli).

¹ Shanghai University of Traditional Chinese Medicine, Shanghai, China

Submitted: February 8, 2022. Revised: June 26, 2022. Accepted: August 29, 2022.

Corresponding Author:

Huayuan Yang, Shanghai University of Traditional Chinese Medicine, Shanghai 201203, China.
Email: yhy4@shutcm.edu.cn



Introduction

In Traditional Chinese Medicine (TCM), qi and blood are transferred to and from the internal organs and meridians at a special spot in the body, known as the acupoint. This phenomenon closely interacts with, responds to, and treats the internal organs and meridians as well as tissues and organs to a certain extent¹. The receptors present in the skin, muscles, and internal organs can be activated by the mechanical, thermal, or chemical stimulation of the acupuncture points, such as moxibustion, injection, and thread embedding². The stimulation signals are then transmitted to the relevant peripheral or central nerves for integration, thereby regulating nerve function, improving local circulation, and inhibiting the release of inflammatory factors, which enhance immunity and also improve body function.

Physiochemical stimulation of acupoints has been widely used to treat acute, chronic, and intractable diseases^{3,4}, such as inflammatory diseases⁵ and neuropathic pain³. In acupoint stimulation, the major problem is its non-modulation, such as the time of acupuncture, dosage, and tools for acupoint injection, and singularity of the acupoint embedding materials, which are needed to be solved urgently. Numerous studies showed that glucocorticoids could play an essential role as an anti-inflammatory analgesic for the treatment of sciatica; however, dexamethasone (DXM) is still the main choice for treating sciatica^{6,7}. The physical stimulation of acupoints in combination with DXM also showed good clinical results in pain management. P2X4R played an important role in neuropathic pain, showing a clear effect on the developmental maintenance of nociception^{8,9}.

Acupoint Catgut Embedding Therapy (ACET) is a kind of the physiochemical stimulation therapy of acupoint, which is often used for the treatment of chronic diseases and exhibits several advantages, including long-lasting stimulation, fewer treatments, and improved compliance as compared to the ordinary acupuncture. However, some of the disadvantages of this therapy included its inability to carry drugs, fast degradation time, the requirement of multiple injections for stimulation, and poor controllability. The most commonly used clinical material for ACET is catgut (sheep intestine thread). However, some patients are allergic to catgut; therefore, other polymeric materials are also developed and applied, having great potentials^{10,11}.

Hydrogels with a three-dimensional (3D) network structure of polymer materials have gradually become a preferred choice for ACET. The *in-situ* injectable hydrogels, which are a new type of embedding material and drug carrier with controlled release, show a temperature-induced sol-gel transition for achieving the long-lasting stimulation of acupoints. However, the existing *in-situ* injectable hydrogels lack certain controllability and have responsiveness and dose adjustability, easily causing internal extrusion and reducing the efficacy in the stimulation of acupoints. Chitosan hydrogel is one of the most widely used bio-compatible natural hydrogels used in genetic engineering^{12,13} and drug release^{14,15}.

It possesses anti-inflammatory, anti-bacterial, and good mechanical as well as adhesive properties. DXM is eliminated rapidly, thereby requiring high and frequent doses, which cause side effects, such as affecting the glucose and cortisol homeostasis¹⁶. These adverse effects can be overcome by the sustained release of drugs using hydrogel.

Smart hydrogels, which respond to external stimuli, such as pH^{17–19}, temperature^{20,21}, and magnetic field^{22,23}, have been widely used in the pharmaceutical industry. In order to enhance the responsiveness of hydrogel material for improving the effects of physiochemical stimulation of acupoints, the hydrogels can be loaded with superparamagnetic Fe₃O₄ nanoparticles, giving them the properties of spatial control, rapid magnetic response, and non-invasive remote actuation. Using the external magnetic field^{24–26}, a certain amount of pressure is exerted on the acupoint, producing the vibration effects similar to physiotherapy. Recent studies showed that chitosan threads were absorbed by the body and produced longer physiological and biochemical responses for up to 20 days or longer²⁷ in the acupoints and surrounding tissues. Therefore, the chitosan hydrogel, showing a certain degree of magnetic responsiveness, has become the focus of the studies.

In the current study, a CS/GP/Fe₃O₄/DXM hydrogel, which was a DXM-loaded injectable *in-situ* thermal cross-linking magnetic responsive hydrogel, was developed for the physiochemical stimulation of acupoint for suppressing pain in the sciatica rat models. The efficiency of this hydrogel was assessed by analyzing the expression levels of two proteins, including P2X4R and downstream p-p38MAPK, in the spinal cord dorsal horn of CCI rats at the acupuncture point ST36.

Material and Method

Preparation of Hydrogels

A CS/GP/Fe₃O₄/DXM hydrogel was prepared by adding 200 mg CS (deacetylation degree of 90%–95%, median molecular weight, Aladdin, Shanghai, China) to 10 mL hydrochloric acid solution (0.1 mol/L) under continuous magnetic stirring for 2 h. Subsequently, to this solution, 2 mL GP solution (56% w/v, Shanghai, Aladdin, China) and 20 nm Fe₃O₄/CS/GP hydrogel, containing 0.3% w/v Fe₃O₄ (Beijing Deke Daojin Science Technology Co. Ltd, China) were added at 25°C. Then, 12 mg DXM (Aladdin, Shanghai, China) was then dissolved in the prepared Fe₃O₄/CS/GP solution. For the control group, the DXM drug (1 mg/mL) was dissolved in a phosphate-buffered saline solution (PBS, pH = 7.4).

Physical Characterization and Gelation of Hydrogel

The liquid hydrogel was converted into gel at 37°C in the 5-ml centrifuge tubes. The gel was then placed in liquid nitrogen for 5 min and lyophilized at –40°C in a freeze-dryer

for 48 h. After freeze-drying, the hydrogel was cut into small pieces (5 mm × 5 mm × 5 mm) and attached to the scanning support using conductive adhesive. Vacuum gold sputter was carried out on the sample pieces for 300 s. The hydrogel samples were observed under the field emission scanning electron microscope (SEM, 250FEG, Quanta, America). The formation of gel was tested using simple the vial-inverting method at a controlled temperature (37°C)²⁸. The vial was inverted for 30 s to ensure the complete transformation of liquid hydrogel into a gel.

Rheological Properties of Hydrogels

After preparing the CS/GP hydrogel, the rheological properties of the gel were determined using an advanced rheometer (MCR101, Anton Paar, Austria). Variations in the storage modulus (G') and loss modulus (G'') with angular frequency, ranging from 0.1 to 100 rad/s, were set after 5 min of solid gel formation at 37°C. A dynamic time sweep test was performed on the CS/GP/Fe₃O₄/DXM hydrogel to determine the gel time of the sample in the physiological state. The parameters were set as follows: 2.0 rad/s frequency, 2% strain, and 37°C temperature.

Swelling Test and Biodegradability

The weight (W_0) of the dried samples of CS/GP hydrogel and CS/GP/Fe₃O₄/DXM ($n = 3$ for each type of hydrogel) was determined. The samples were rehydrated in PBS for 20, 40, 60, 80, and 120 min at 37°C. After their removal from PBS, the swollen hydrogels were dehydrated using filter paper and again weighted (W_t). The swelling rate of the hydrogels was calculated using Eq. (1).

$$\text{Swelling (\%)} = (W_t - W_0)/W_0'100\% \quad (1)$$

The dried CS/GP and CS/GP/Fe₃O₄/DXM hydrogels ($n = 3$ for each hydrogel) were incubated at 37°C in 20 mL PBS, containing 500 µg/mL lysozyme, in a shaking incubator at 50 rpm for 3, 6, 9, 12, and 15 days. The control group was incubated in PBS without lysozyme. All the samples were weighed before (W_0) and after incubation (W_t) for different durations. The sample degradation was calculated using Eq. (2).

$$\text{Degradation (\%)} = (W_t - W_0)/W_0'100\% \quad (2)$$

In-vitro Study of Drug Release

The drug release testing of DXM-loaded hydrogel was performed using a dialysis bag (molecular weight cut off, MWCO: 10000 Da). The hydrogel-containing dialysis bag, after gel formation, was incubated in 25 mL PBS (pH 7.4) at 37°C and 50 rpm in a thermostatic shaker. A 5-ml PBS solution was replaced regularly after 4, 8, 24, 48, 72, 120, and

192 h with the same volume of PBS each time (three samples were taken at each time point and the experiments were triplicated). The amount of DXM released in each sample was analyzed using a UV spectrophotometer (UV-2102C, Unice, China).

In-vitro Cytotoxicity Assay of CS/GP/Fe₃O₄/DXM Hydrogel

The cytotoxicity of CS/GP/Fe₃O₄/DXM hydrogel was evaluated using Cell Counting Kit-8 (CCK-8, SAB, USA) assay. A 100-µL L929 cell suspension was plated into each well of the 96-well plate with a cellular density of 5×10^4 /mL and incubated in an incubator, containing 5% CO₂ concentration, at 37°C for 24 h. Then, 100 µL of CS/GP/Fe₃O₄/DXM hydrogel extracts was added to each well, and co-cultured with cells. The samples were then incubated in a CO₂ incubator at 37°C for 24 h. As a control group, the cells without magnetic hydrogels were used. After incubating with CCK-8 at 37°C for 1 h, the cellular morphologies were photographed using a microscope (XDS-500C, Caikon, China) and their optical density (OD) values at 450 nm were measured using a microplate reader (DNM-9602, Perlong, China). Then, the cell viability of each sample was calculated.

Animals and Surgical Preparation

Healthy male SD rats, weighing 200 ± 20 g, were used for the implantation of the hydrogel samples. For the establishment of the CCI rat model, the SD rat models were fasted 1 d before modeling and then anesthetized with isoflurane gas. The middle of the right posterior leg of the rat was sterilized and a sterile towel was laid down. About 2 cm of their skin was cut open and the biceps femoris muscle was bluntly separated, exposing the middle segment of the right sciatic nerve. The ligature was loosely ligated with the four stitches of 4-0 silk thread, having a 1-mm distance between two stitches. The tightness was kept appropriate to make the ligature slide over the sciatic nerve trunk, leading to a slight trembling of the rat's muscles. After establishing the rat models, the vital signs and wound healing of the rats were closely observed.

Experimental Groups and Treatments

A total of 56 healthy male rats were divided into seven groups, including control, CCI, catgut, CS/GP, CS/GP/Fe₃O₄, CS/GP/Fe₃O₄/DXM, and DXM groups. A 30-cm magnetic field with a magnetic field strength of 0.4 T was set next to the rat's ST36 acupoint. The rats were treated twice daily for 30 min with an interval of 6 h between the two treatments (10:00–10:30 and 16:00–16:30). The CS/GP, CS/GP/Fe₃O₄, and CS/GP/Fe₃O₄/DXM groups were treated by the intramuscular injection of the respective hydrogels (0.1 ml) at the ST36 acupoint in the SD rats. DXM (0.1 mg) was injected per acupoint. The catgut group was implanted with

2-mm catgut (Shandong Boda medical supplies Co., Ltd, China). Each treatment group of rats was treated weekly.

Finite Element Simulation of the Magnetic Responsiveness

The correlations between the magnetic force at the free end of the magnet and the gap between the hydrogels were measured using the finite element method *in-vitro*. The maximum value of the magnetic force was also calculated. The hydrogels had a gap distance of 8 mm to 0 mm, and the hydrogels were designated as homogeneous or ellipsoidal spheres.

The ST36 acupoint is located near the tibialis anterior muscle. Therefore, the hydrogel was injected into the muscle layer. The finite elements were used to simulate the stretching force on the muscles near the acupoint. Using the NdFeB, the simulated magnetic field was 75 mm × 75 mm × 25 mm with a magnetic field strength of 0.4 T. The hydrogel samples were fixed next to the muscle or at one end of the muscle. In order to evaluate the effects of magnetic stimulations on the muscles, a simplified simulation was performed using the Finite Element Software (COMSOL Multiphysics 6.0, Sweden). The muscle was measured as a fusiform cylinder as well as Young's modulus of 30 kPa and Poisson's ratio of 0.45²⁹. A force was applied at the surface as a force boundary condition. The strain distribution within the muscle was measured.

Behavioral Testing

The paw mechanical withdrawal threshold (PMWT) : The right hind paw of the SD rat was measured using a paw nociceptive Electronic Von Frey tester (IITC 2391, USA) before surgery and on the 1st, 3rd, 5th, 7th, 10th, and 14th day of surgery. The SD rats were placed in cages on a wire panel with a mesh for 30 min. When the rats were quiet, a gradual pressure was applied to the right hind paw until the rats showed movements, such as lifting, avoiding, or licking the foot. The maximum pressure applied to the right hind paw at the time of a positive response was recorded and repeated three times at an interval of 5 min.

Hematoxylin and Eosin (H&E) Staining and Enzyme Linked Immunosorbent Assay (ELISA)

The formation and compatibility of the hydrogels were evaluated in the SD rats *in-vivo*. The skin on the back of the SD rat was fixed in 10% paraformaldehyde for 2 days. After the skin tissues were made transparent using xylene, they were dehydrated and embedded in paraffin, followed by cutting into 5- μ m-thick sections. The sections were dewaxed in xylene, rinsed with water, and stained with H&E under a light microscope (ECLIPSE Ni, Japan) in order to observe the histopathological changes in the skin.

In order to evaluate the inflammatory response, ELISA was performed to detect the expression levels of serum TNF- α ,

IL-6, and IL-1 β in rats. The rats were anesthetized on the 14th day of surgery using 1 mL/100 g of 0.3% pentobarbital sodium. The rats' tissues and organs were bluntly separated to expose the abdominal aorta. A total of 5 mL of blood was collected from the abdominal aorta and centrifuged at 3000 rpm for 15 min at 4°C. Then, the blood serum was collected. The expression levels of serum TNF- α , IL-6, and IL-1 β were determined using their respective ELISA kits (Xinyu, Biotech, Shanghai, China) following the manufacturer's instructions.

Western Blotting

Western blotting was performed to determine the protein expression levels of P2X4R, p38MAPK and p-p38MAPK in the L4-L6 dorsal horn of the spinal cord. The four rats from each group were anesthetized on the 14th day of surgery and the L4-L6 segments of the spinal cord were removed. After further fragmentation by ultrasound, the tissues were placed on ice for 30 min and then centrifuged at 4°C for 20 min at 15,000 rpm. The supernatant was extracted, and the protein concentrations were determined using the bicinchoninic acid (BCA) method. The extracted proteins (50 μ g) were denatured in a loading buffer at 95°C for 5 min and separated on a 12% sodium dodecyl-sulfate (SDS)-polyacrylamide gel. The samples on SDS-polyacrylamide gel were then transferred onto a polyvinylidene fluoride (PVDF) membrane, which was then probed with the primary antibodies at 4°C overnight. The primary antibodies included rabbit anti-P2X4R (1:1000, CST, USA), rabbit anti-p38MAPK (1:1000, CST, USA), and rabbit anti-p-p38MAPK (1:1000, CST, USA). Then, the excess antibodies were washed with TBST buffer thrice for 5 min. The membrane was incubated with the respective horseradish peroxidase-conjugated secondary antibodies (1:1000) at room temperature for 1 h, followed by washing similar to the previous step. ECL luminescent solution was prepared, and the images were captured using a GE luminometer (Tanon-5200, Shanghai, China) and analyzed using Image J software for the image gray value analysis.

Quantitative Real-Time PCR

Total RNA was extracted from the spinal cord L4-L6 tissues and converted into cDNA. Real-time PCR was performed using an iCycler (ABI-7300), SYBR Green supermix (Thermo, #K0223), and 4 ng of the cDNA³⁰. For PCR, the primers were synthesized by Invitrogen (Fermentas, #K1622). The primers for the *P2X4R* gene were as follows; forward primer 5'-CATCCTCCCCAACATCAC-3' and reverse primer 5'-CCCTCAACTGCCATCTCC-3.'

Statistical Analyses

All the experimental data were statistically analyzed using SPSS 26.0 (Statistical Package of Social Science, Chicago, USA) software and plotted using GraphPad Prism (version 5.01, GraphPad Software, San Diego, USA). The bivariate

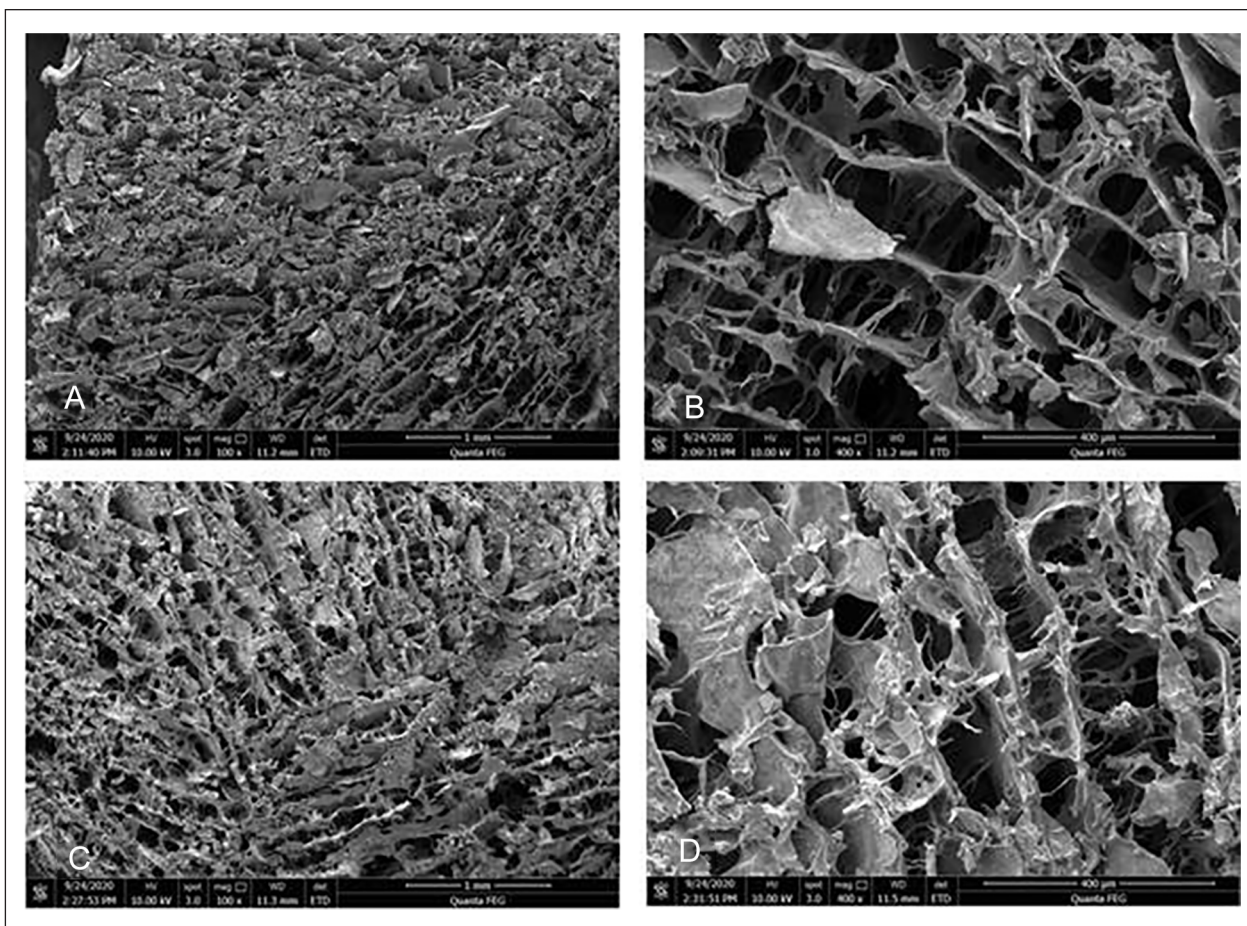


Figure 1. Microscopic characterization of the thermosensitive hydrogel. (A and B) SEM pictures (X100, X400) of the CS/GP hydrogel showed that the gel carrier contained a loose porous network matrix structure with a smooth matrix surface; (C and D) CS/GP/Fe₃O₄/DXM hydrogel had also a loose porous network matrix structure because the Fe₃O₄/DXM was embedded on the surface or inside of the matrix, which was rough and granular.

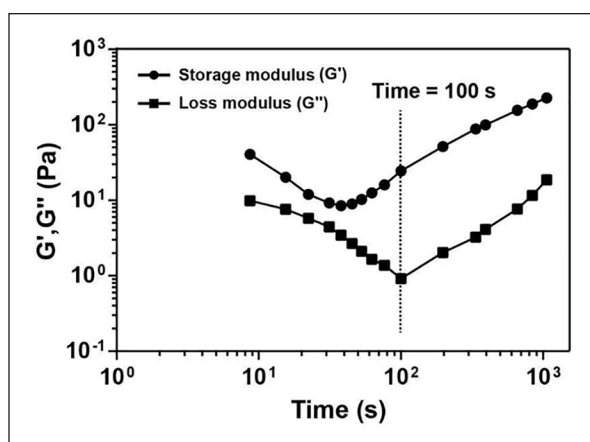


Figure 2. The gel-forming properties of hydrogels. Variations in the storage and loss moduli (G' and G'', respectively) with time at 37°C.

analysis of variance (ANOVA) and Bonferroni post hoc tests were used for comparing the threshold of mechanical pain at different time points in each group. For the comparison of

seven groups, one-way ANOVA was performed for the analysis of biochemical indicators. All the numerical data were expressed as means \pm SEM. The statistical significance was set to $P < 0.05$.

Results

Characterization of Hydrogels

After freeze-drying the hydrogels, SEM revealed that the structure of hydrogel was a 3D loose porous network (Fig. 1), which facilitated the sustained release of DXM and exchange of nutrients/wastes. Evaluating the gel-forming properties of hydrogels showed the formation of gel immediately at 37°C, and the state of the gel changed in a time-dependent manner (Fig. 2). The difference between the storage modulus and the loss modulus of the hydrogel was small until 100 s, indicating that the hydrogel was semi-solid at this stage. However, after 100 s, the storage modulus was always much higher as compared to the loss modulus, indicating that the hydrogel was completely transformed into a solid state. Therefore, all the

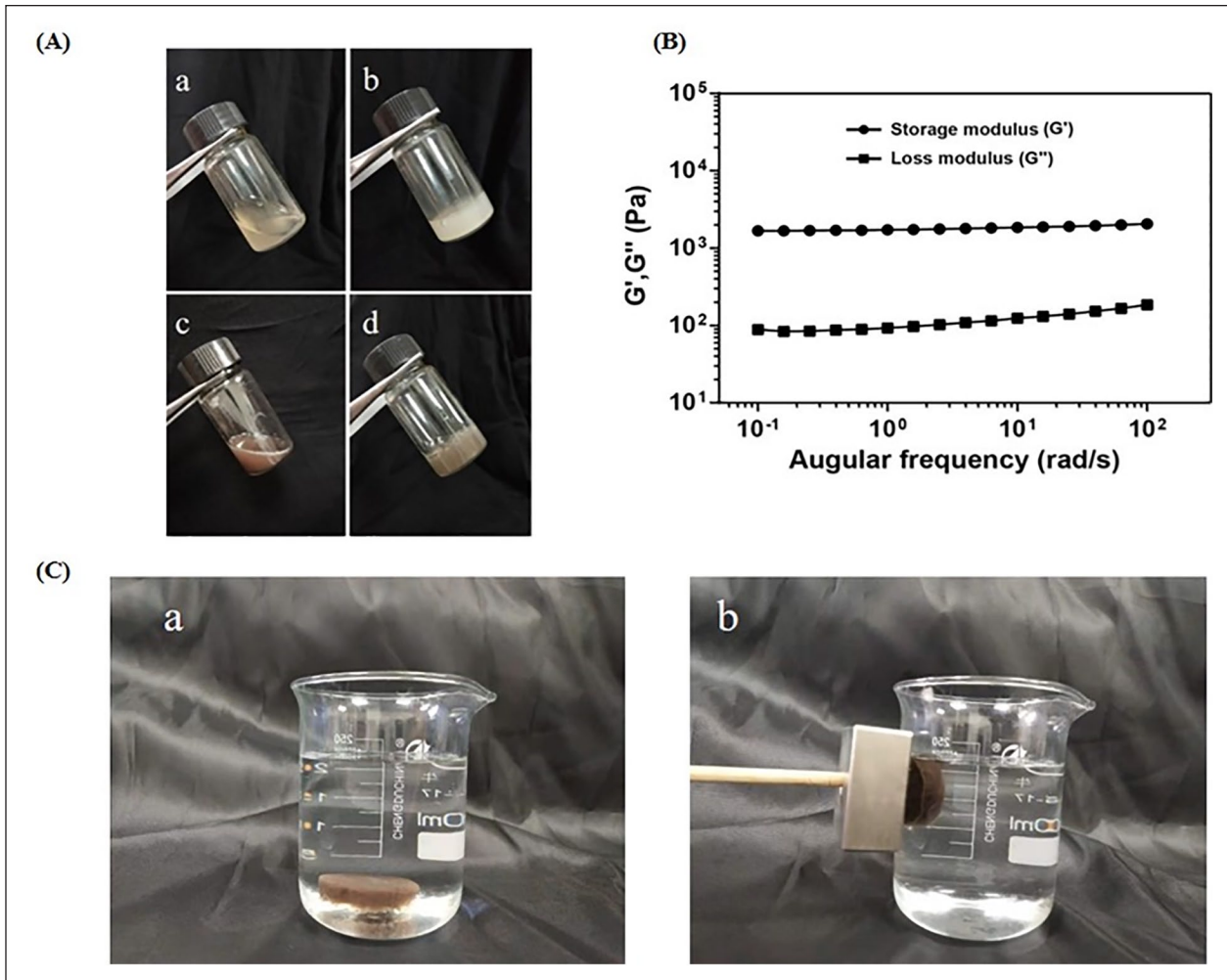


Figure 3. Thermosensitive and magnetic responsiveness of hydrogels. (A) Photographs of the (a and b) CS/GP hydrogel at 25°C and 37°C, and (c and d) CS/GP/Fe₃O₄/DXM hydrogel at 25°C and 37°C; (B) Variations in the storage and loss moduli (G' and G'', respectively) with angular frequency at 37°C; (C) Photographs of the (a) CS/GP/Fe₃O₄/DXM hydrogel sunk to the bottom of beaker with saline and (b) CS/GP/Fe₃O₄/DXM hydrogel attracted to the left of beaker having a 0.4-T magnetic field. The arrows indicate the direction of motion of CS/GP/Fe₃O₄/DXM hydrogel.

tests were performed after 5 min of gel formation to ensure the complete formation and stability of the gel.

The CS/GP hydrogel was present in the form of a yellow transparent liquid at room temperature (25°C), while the CS/GP/Fe₃O₄/DXM hydrogel appeared as a black liquid (Fig. 3A). The solution state of the hydrogels facilitated the injectability of hydrogels; all the hydrogels could be injected using a syringe. These *in-situ* liquid solutions could transform from sol to gel at physiological temperature (37°C). Fig. 3A(a), A(b) showed that the CS/GP was a pale yellow transparent liquid at room temperature, showing good fluidity, and the liquid level changes with the tilting of the test tube. After heating in a water bath for 5 min above 37°C, the CS/GP liquid rapidly transformed into a gel, adhering to the wall of the test tube and appearing as a milky yellow, homogeneous, turbid, and opaque gel, as well as lost fluidity when the test tube was

tilted. Fig. 3A(c), A(d) showed that the CS/GP/Fe₃O₄/DXM hydrogel appeared as a black liquid at room temperature with good fluidity and the liquid level changed with the tilting of the test tube. However, after heating the gel in a water bath for 5 min above 37°C, the gel transformed into a black solid gel without fluidity when the test tube was tilted. In order to demonstrate the sol-to-gel transition, a rheology test was performed. As illustrated in Fig. 3B, the G' was much higher than the G'' at 37°C, clearly indicating the gelation, which enabled the hydrogel to adhere to the acupoints. The results of magnetic responsiveness showed that when the CS/GP/Fe₃O₄/DXM hydrogel was placed in a beaker with saline solution, the hydrogel sank to the bottom of the beaker. After giving a magnetic field of 0.4-T magnetic field strength, the hydrogel was attracted to the left side of the beaker, thereby showing its good magnetic targeting potential *in-vitro* (Fig. 3C).

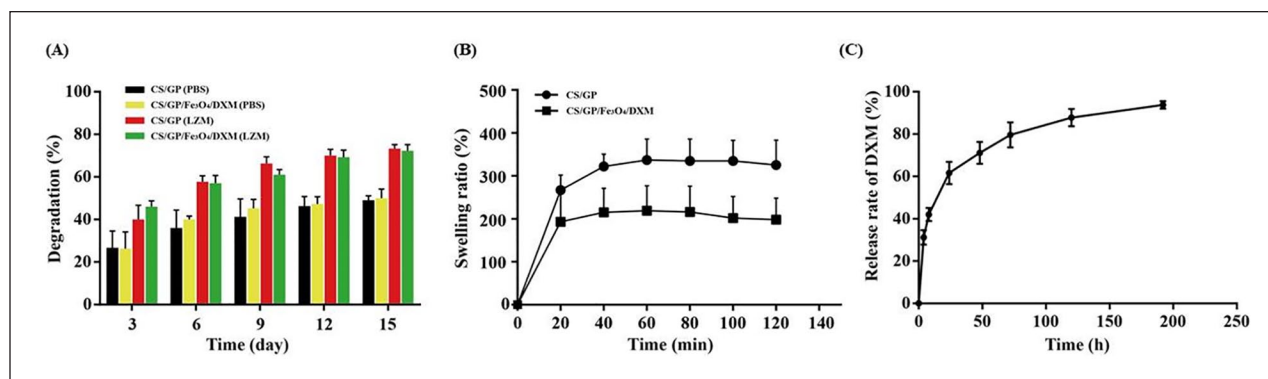


Figure 4. Degradation, swelling, and drug release of the hydrogels. (A) Degradation degree of the CS/GP, CS/GP/Fe₃O₄/DXM hydrogels with and without LZM; (B) Swelling ratio; and (C) Release curve of the DXM from CS/GP/Fe₃O₄/DXM hydrogel *in-vitro*. All the data are expressed as mean \pm SEM, n = 3. Abbreviation: LZM, lysozyme.

The *in-vitro* degradation of hydrogels was studied by simulating them with lysozyme. The control group was simulated with a media, containing PBS. The degradation rate of all the hydrogels increased with the increase in the incubation time. Both the CS/GP and CS/GP/Fe₃O₄/DXM hydrogels showed no significant differences in their degradation degree and trend over time as compared to the control group (Fig. 4A). The degradation rates of hydrogels in the medium with and without lysozyme were different. The incubation of hydrogels with lysozyme over the 2-week incubation period showed a relatively rapid degradation rate in the first 3 days, which slowed down thereafter. The degradation rate could reach roughly 60% by day 6 and reach about 80% on day 15 for both the CS/GP and CS/GP/Fe₃O₄/DXM hydrogels incubated with lysozyme. As compared to the hydrogels incubated with lysozyme, those incubated with PBS showed a little difference in their degradation rates during the first 3 days. However, the increase in the degradation rate was much slower, reaching nearly 50% on day 15 for both the hydrogels. These results indicated that the CS/GP hydrogel had a relatively acceptable degradation rate and could be applied for the prolonged stimulation of acupoints, having magnetic responsiveness and drug-loading abilities.

The swelling ratios of the hydrogels were assessed in PBS (pH 7.4) at 37°C in a shaking incubator. As shown in Fig. 4B, the CS/GP and CS/GP/Fe₃O₄/DXM hydrogels reached the swelling ratios of nearly 280% and 180%, respectively, after 20 min. Their swelling ratio gradually and slowly increased for 60 min, reaching the swelling equilibrium within 1 h with the steady swelling ratios of nearly 300 and 200% for the CS/GP and CS/GP/Fe₃O₄/DXM hydrogels, respectively. All the hydrogels were maintained in the gel-forming state at 37°C during the period of the test. The swelling ratio of CS/GP/Fe₃O₄/DXM hydrogel was much lower than that of the CS/GP hydrogel, probably due to the space occupied by Fe₃O₄/DXM, which was related to the controlled release of the drug.

The drug release tests of the CS/GP/Fe₃O₄/DXM hydrogel were performed in a 25-mL PBS (pH 7.4). The controlled

drug release experiments were observed after 5 min of the formation at 37°C in a thermostatic shaking incubator. The CS/GP/Fe₃O₄/DXM hydrogel showed a sustained release of the drug (DXM) (Fig. 4C). In the first 4 h, the CS/GP/Fe₃O₄/DXM hydrogel released a total of 31.22% of the DXM, which reached 42%, 62%, 71%, 80%, and 88% after 8 h, 24 h, 48 h, 72 h, and 120 h, respectively. The release curve plateaued after 192 h.

Injectable CS/GP/Fe₃O₄/DXM Hydrogel Attenuated PMWT After CCI Model

Among the seven groups, the baseline measurements of the PMWT using the Electronic Von Frey tester did not show differences. After the constriction of the unilateral sciatic nerve, the established CCI rats developed evident tactile allodynia in 1 day in their ipsilateral hind paw, which persisted for about 14 days. The PMWT in the control group remained stable for 14 days. The *in-situ* injection of CS/GP/Fe₃O₄/DXM hydrogel at the ipsilateral acupoint (ST36) increased the PMWT on day 1 and showed significant improvements after 14 days. Moreover, as compared to the control group, the PMWT of CS/GP/Fe₃O₄ and DXM groups improved and there was no obvious difference between the CS/GP and CCI groups. Two-way ANOVA revealed that the CS/GP/Fe₃O₄/DXM treatments showed significant improvements (Fig. 5).

Formation and Biocompatibility of the CS/GP and CS/GP/Fe₃O₄/DXM Hydrogels *in-vivo*, and Cytotoxicity of CS/GP/Fe₃O₄/DXM Hydrogel *in-vitro*

The pre-gels of CS/GP and CS/GP/Fe₃O₄/DXM hydrogels were subcutaneously injected into the dorsal regions of the SD rats to evaluate the toxicities of the *in-situ* hydrogels. The physiological temperature of the SD rats was about 37°C. Therefore, the hydrogels could form on their backs and showed adherence to the surrounding tissues (Fig. 6A1–A4).

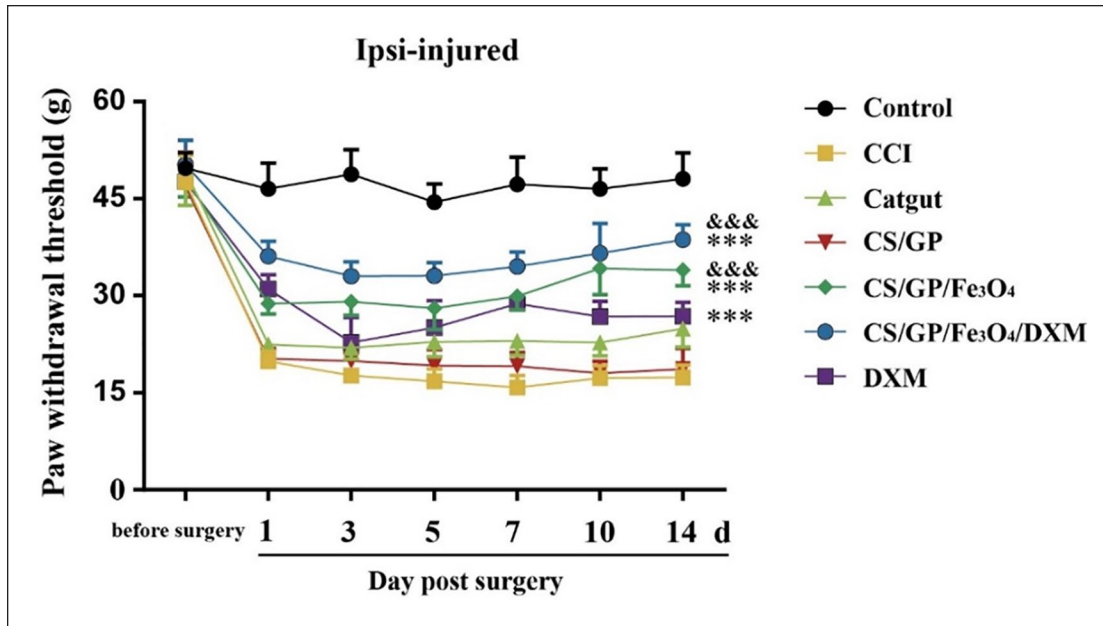


Figure 5. PMWT of the CCI rats was measured using Electronic Von Frey tester. CS/GP/Fe₃O₄/DXM hydrogel significantly reduced allodynia as shown by the increase in PMWT. The data were expressed as the means \pm SEM ($n = 8$ for each group). * $P < 0.05$, as compared to the CCI group, and [&] $P < 0.05$ as compared to the catgut group. Abbreviations: CCI, chronic constriction injury of the sciatic nerve; PMWT, paw mechanical withdrawal threshold.

The inflammatory responses, such as local redness, swelling, or necrosis were not observed, indicating no *in-situ* toxicity of the hydrogels. Moreover, the CS/GP solution could form gels *in-situ* thereby ensuring the ability for the continuous stimulation of acupoints. The gel formation was also confirmed by the H&E staining, showing well-demarcated and fixed gels in the rats (Fig. 6B, C). The magnetic nanoparticles (MNPs) remained encapsulated in the hydrogels and no necrosis was observed in the tissue surrounding. Clear boundaries could be observed on the skin tissue around the injection site of hydrogels. The results indicated that these hydrogels had good biocompatibility and facilitated the use of acupoints injection in the rats. The CCK-8 results suggested that there was no significant difference in the cell survival between the CS/GP/Fe₃O₄/DXM hydrogel and control groups ($P > 0.05$). Meanwhile, the *in-vitro* cytotoxicity tests showed that CS/GP/Fe₃O₄/DXM hydrogel was essentially non-cytotoxic (Fig. 7).

Magnetic Force Could Be Used as a Physical Stimulation of Acupuncture Points *in-vivo*

The maximum value of *in-vitro* magnetic force by finite element simulation was 24 N, demonstrating the controllability of the magnetic field strength. The strain generated using 24 N magnetic field strength on the left end of the muscle was 0.18%. The strain distribution was smaller in the middle of muscles and larger on both sides. The results showed that stretching the muscles by applying magnetic force to one end of the muscle could be used as a physical stimulation of the

acupuncture points, which was similar to the acupuncture stimulation of the acupoint. The magnitude of the magnetic force increased by increasing the concentration of magnetic nanoparticles and the strength of magnetic field, thereby increasing the intensity of the stimulus (Fig. 8).

Injectable CS/GP/Fe₃O₄/DXM Hydrogel Could Attenuate the Overexpression of TNF- α , IL-6, and IL-1 β in Serum After the CCI Model

The serum expression levels of TNF- α , IL-6, and IL-1 β were detected using ELISA. These expression levels in the CCI group and CS/GP group significantly increased as compared to those in the control group ($P < 0.001$, Fig. 9). However, these expression levels decreased significantly by the CS/GP/Fe₃O₄ and CS/GP/Fe₃O₄/DXM hydrogels as compared to those in the CCI group. Furthermore, as compared to the control and CS/GP groups, the catgut and DXM groups also showed a decrease in their expression levels. The CS/GP/Fe₃O₄ and CS/GP/Fe₃O₄/DXM groups also showed a reduction in their expression levels, these reductions were lower than those of the catgut and DXM groups. These results indicated that CS/GP/Fe₃O₄/DXM hydrogel could inhibit the neuropathic pain systemic immune response by lowering the expression levels of TNF- α , IL-6, and IL-1 β in serum with the continuous drug release and magnetic stimulation. These effects were superior to the drug injection and catgut alone without drug-carrying properties, thereby showing the good anti-inflammatory and analgesic effects of CS/GP/Fe₃O₄/DXM hydrogels in the CCI rats at the ST36 acupoint.

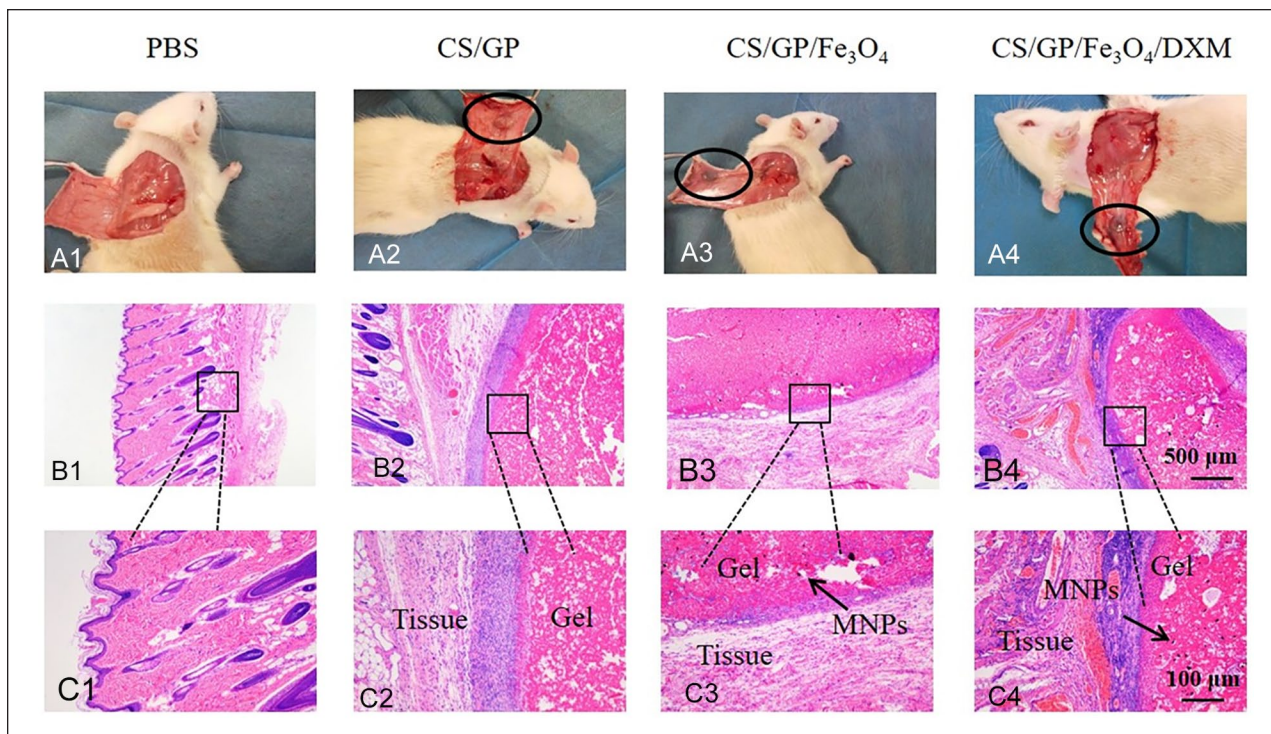


Figure 6. Biocompatibility of the hydrogels *in-vivo*. (A) Representative images of the dorsal skin of the SD rats injected with 200 μL of PBS, CS/GP, CS/GP/Fe₃O₄, and CS/GP/Fe₃O₄/DXM hydrogels for 14 days. (B) Small and medium boxes indicate the hydrogels formed in the dorsal skin of the SD rats. (C) Magnified images around the small boxes. The black arrow shows MNPs (magnetic nanoparticles).

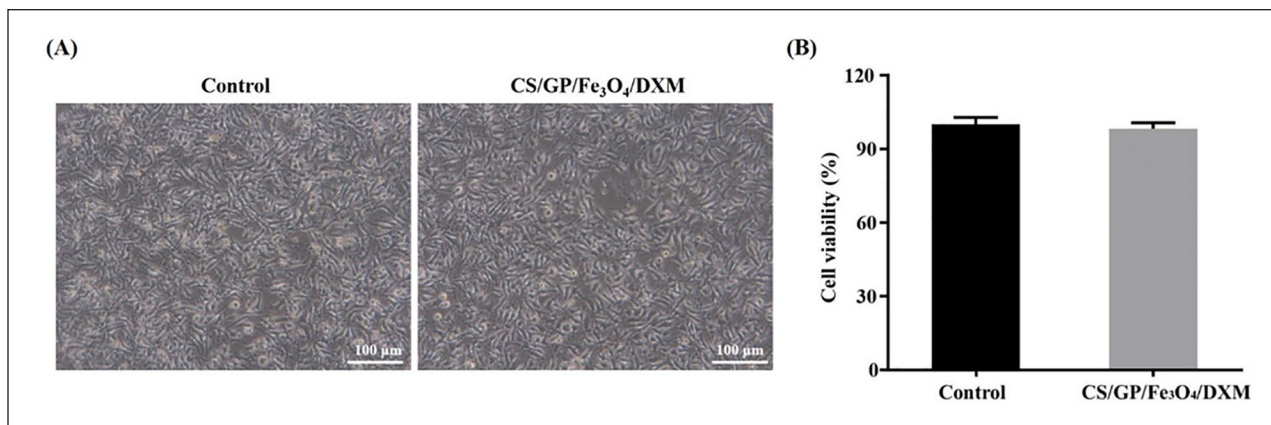


Figure 7. Cytotoxicity of CS/GP/Fe₃O₄/DXM hydrogel *in-vitro*. (A) Microscopic images of L929 fibroblasts co-cultured with CS/GP/Fe₃O₄/DXM hydrogel for 24 h. (B) Cell viability after the co-culturing of cells with CS/GP/Fe₃O₄/DXM hydrogel for 24 h.

Injectable CS/GP/Fe₃O₄/DXM Hydrogel Could Reduce the Overexpression of P2X4R Expression and p-p38MARK Protein Expression in the CCI rats

The PCR results indicated that the injection of CS/GP/Fe₃O₄ and CS/GP/Fe₃O₄/DXM hydrogels showed a significant reduction in the elevated *P2X4R* expression levels in the CCI rats on Day 14 ($P < 0.05$ and $P < 0.01$). The catgut therapy and DXM injection also reduced the *P2X4R* expression

levels in the CCI rats, while the injection of CS/GP hydrogel showed no effects (Fig. 10D). As compared to the catgut therapy, the CS/GP/Fe₃O₄/DXM hydrogel could significantly decrease the *P2X4R* expression levels ($P < 0.001$). These results indicated that *P2X4R* was involved in the effects of CS/GP/Fe₃O₄/DXM hydrogel on the CCI rats. Western blot analysis also showed similar results at the *P2X4R* protein level as well as for the p-p38MARK protein expression (Fig. 10A–C). These findings indicated that the

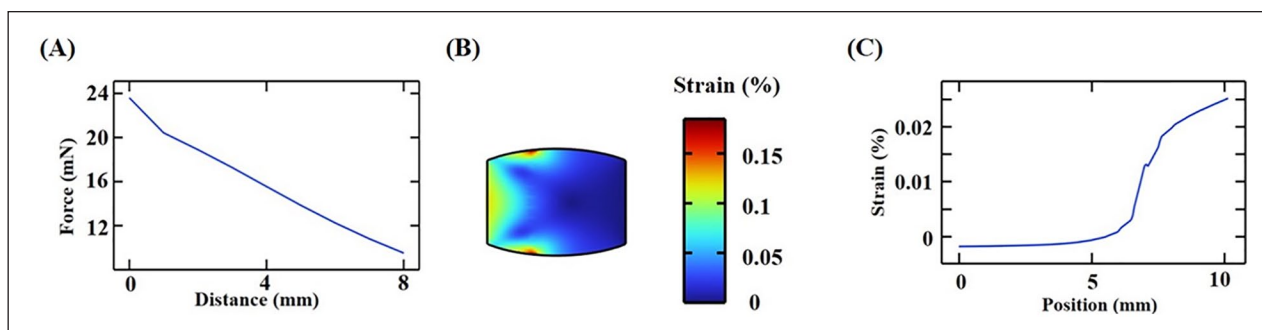


Figure 8. Finite element simulation of the magnetic responsiveness. (A) Magnetic force varied with the distance between the free end of the magnet and magnetic hydrogel *in-vitro*. (B) Strain distribution estimated by the finite element simulation was stretched along the left side of the muscle. (C) Strain distribution along the muscle centerline: the normal component strain resolved into a component in the vertical direction.

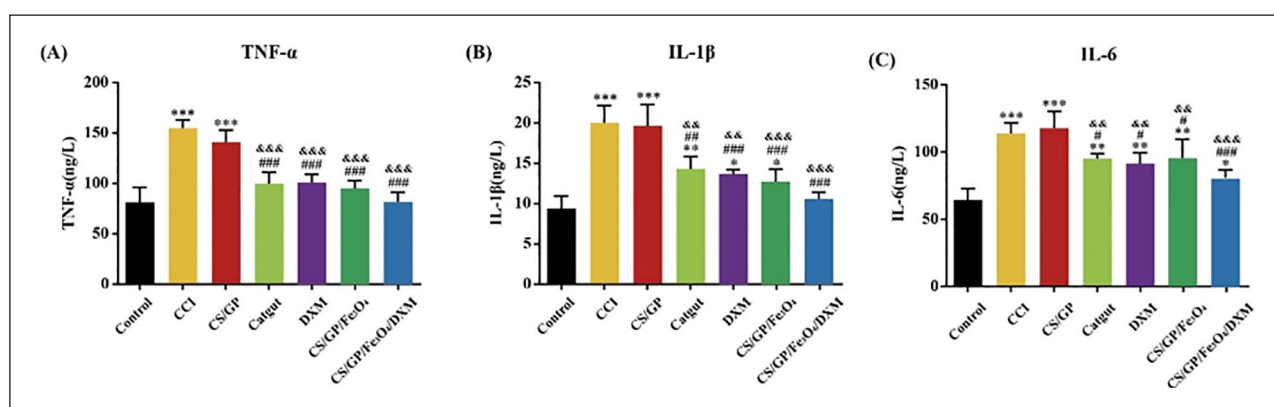


Figure 9. Role of the pro-inflammatory mediators in the effects of CS/GP/Fe₃O₄/DXM hydrogel on the CCI rat models. (A–C) Expression levels of TNF- α , IL-1 β , and IL-6 in serum. All the data were expressed as the means \pm SEM ($n = 4$ for each group). * $P < 0.05$ as compared to the control group; # $P < 0.05$ as compared with the CCI group; &# $P < 0.05$ as compared to the CS/GP group. Abbreviations: IL-6, interleukin-6; TNF- α , tumor necrosis factor-alpha; IL-1 β , interleukin 1 β .

CS/GP/Fe₃O₄/DXM hydrogel could effectively treat sciatica by down-regulating the expression levels of P2X4R and downstream p-p38 MARK protein in the CCI rats.

Discussion

This study characterized the injectable CS/GP, CS/GP/Fe₃O₄, and CS/GP/Fe₃O₄/DXM hydrogels *in-situ* and evaluated their properties *in-vitro* and therapeutic effects *in-vivo*. The results showed that the CS/GP/Fe₃O₄/DXM hydrogel had good physicochemical properties as well as a superior therapeutic effect as compared to the groups (CS/GP hydrogel, CS/GP/Fe₃O₄ hydrogel, catgut, and DXM treatment) in terms of their inflammatory and analgesic effects in the CCI rats, showing great potential in the physicochemical stimulation of acupoints.

The advantages of the thermosensitive hydrogel include no requirement of surgery, easy availability, and a controllable magnetic field. These advantages make these hydrogels preferred materials for ACET. This study showed that the CS/

GP hydrogels could maintain a liquid state at room temperature, allowing for a dose-controllable injection, improving the tools of ACET, showing the drug- and MNPs-loading properties, and reducing the treatment costs. After injecting into the acupoint, a gel was formed at the physiological body temperature (37°C), which could adhere to the ST36 acupoint and release drugs, thereby exerting a certain magnetic responsive effect on the acupoints. The field strength and concentration of the magnetic fluid were adjustable. The low concentrations of Fe₃O₄ and drug dose used in this study could provide a better therapeutic effect. Chitosan is a widely studied polysaccharide. Although it did not contain thermosensitive polymers, GP could make it a thermosensitive hydrogel, thereby achieving the sol-to-gel transition³¹. Both the chitosan and β -glycerophosphate have good biocompatibilities and can form hydrogel at 37°C³². The gel was formed by electrostatic crosslinking³³. Moreover, the degree of deacetylation and molecular weight of CS could also affect the characteristics of hydrogels³⁴. The DXM and Fe₃O₄ did not influence the thermal crosslinking of hydrogels, ensuring

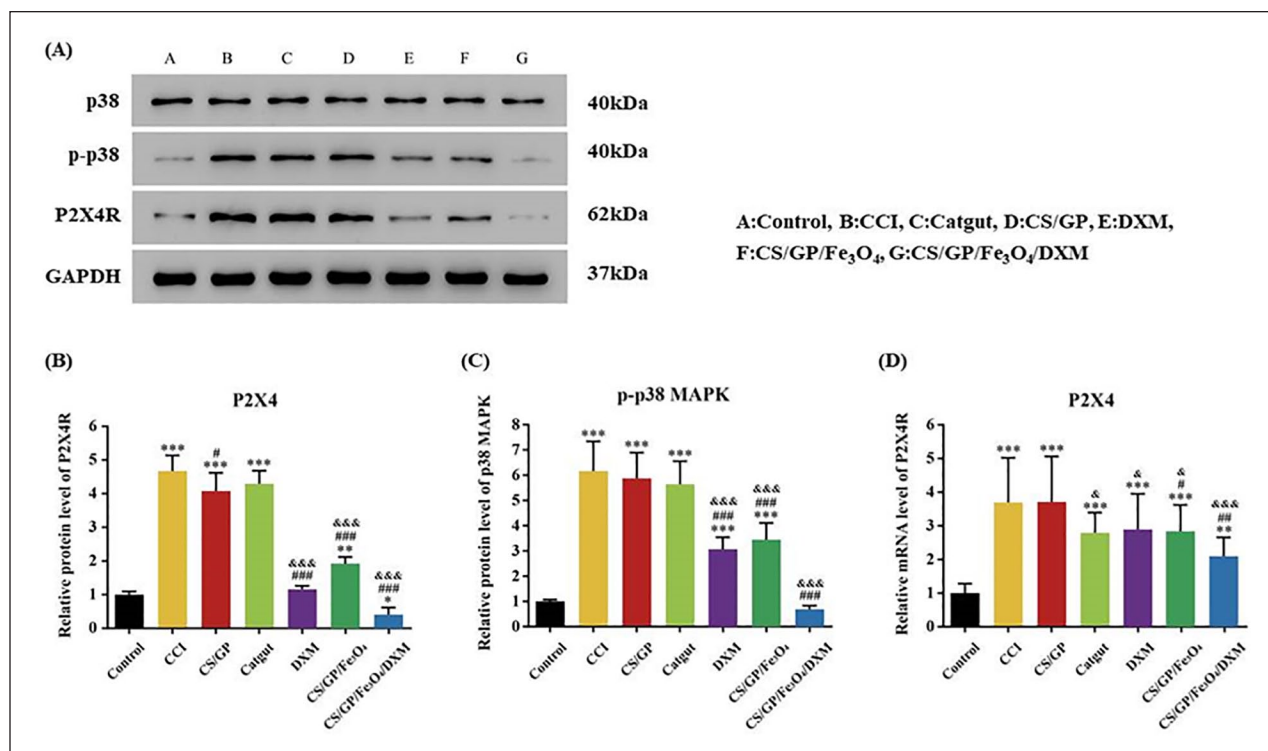


Figure 10. Treatments with the injection of CS/GP/Fe₃O₄/DXM hydrogel could inhibit the P2X4R and p-p38 MAPK protein levels in the dorsal horn of the CCI rats' spinal cord, which was detected using Western blot assay and quantitative real-time PCR. (A) Representative images of the P2X4R and p38MAPK protein levels in the dorsal horn of the spinal cord, p38, and GAPDH were used as a loading control. (B and C) Summary data of the P2X4R and p-p38 MAPK proteins. (D) mRNA levels of the P2X4R in the dorsal horn of the spinal cord. All the data were expressed as means \pm SEM ($n = 4$ for each group). * $P < 0.05$ as compared to the control group; # $P < 0.05$ as compared to the CCI group; and &#x26; $P < 0.05$ as compared to the CS/GP group.

their good stability. These results indicated a promising potential for the *in-situ* applications of hydrogel in the physiochemical stimulation of acupoints.

The CS/GP hydrogel showed great potential in controlling the delivery system for the Fe₃O₄/DXM-loading. In addition, the swelling and degradation properties of the hydrogels might also play an important role in the slow release of drugs. These hydrogels maintained their 3D structure while degrading, thereby facilitating the sustainable release of DXM. Besides, the swelling equilibrium reached within 1 h while maintaining the stability of the hydrogels network and not affecting the drug-controlling and magnetic responsive properties, when subjected to compression or deformation. The release kinetics profile of DXM revealed a burst release in the start, showing the advantages of rapid arrival of effective dose at the target site and relief of inflammatory response after injection at the acupoint. This burst release might be due to the dissolution of the hydrogel surface. Next, the slowed release phase of DXM was related to the degradation rate of hydrogels³⁵. Furthermore, with the widespread applications of magnetic hydrogels²³, their magnetic therapeutic potentials can be used in TCM, which can greatly improve the utilization and function of embedding material. Furthermore, the magnetic field has the advantages

of simple operation, fast response, and high controllability. This study showed that the CS/GP/Fe₃O₄ hydrogel had a better therapeutic effect as compared to the CS/GP hydrogel, which might be due to the weak vibrations produced by Fe₃O₄ under the action of the magnetic field, showing a targeted and weak physiotherapeutic effect of the hydrogel. Considering the risks of adverse effects, the efficacy and targeting ability of DXM could be increased at a given dose while reducing its side effects by the weekly injection of Fe₃O₄-loaded CS/GP hydrogel at the ST36 acupoint. The results showed that the CS/GP/Fe₃O₄/DXM hydrogel provided a continuous release of the DXM, which could be controlled in space and dose. Its efficacy and prospects were far superior to those of the catgut and DXM groups.

CCI is the most common animal model of neuropathic pain, such as spontaneous pain, thermal hyperalgesia, and mechanical hyperalgesia, which appeared in the CCI rats after nerve ligation for 2 weeks and the maximum pain at day 14. Therefore, the CCI model is the best model for simulating the chronic neuralgia symptoms³⁶. ST36 is an important acupoint for the treatment of sciatica³⁷⁻³⁹, which was used in this study. Peripheral nerve injury could elicit a series of inflammatory responses, resulting in nociceptive hypersensitivity with decreasing mechanical pain threshold to the

injurious stimuli. The PMWT increased in the CCI rats of all the CS/GP/Fe₃O₄/DXM, CS/GP/Fe₃O₄, and DXM groups, especially the CS/GP/Fe₃O₄/DXM group, which significantly reduced the mechanical allodynia as compared to the control group.

The expression levels of the inflammatory factors in the serum of CCI rats were elevated, which were mitigated after the injection of CS/GP/Fe₃O₄/DXM hydrogel at the ST36 acupoint. Injury neurons are sensitized by TNF- α , IL-1 β , and IL-6, which are produced by macrophages, mast cells, and neutrophils during the sensitization. IL-1 β and TNF- α are important factors in the nuclear transcription factor-kappa B (NF- κ B)⁴⁰ signaling pathway, which is the first inflammatory response and plays a vital role in promoting inflammation. The current study showed consistent results. A remarkable increase in the expression levels of TNF- α , IL-1 β , and IL-6 was observed in the CCI group, while the CS/GP/Fe₃O₄/DXM group showed a noticeable decrease in the expression levels of these proteins as compared to the catgut group. This might be due to the lack of 3D porous structure in catgut, which could not be loaded with drugs. These results confirmed that the injectable *in-situ* CS/GP/Fe₃O₄/DXM hydrogel with controlled release of the drug and magnetic responsiveness could ease the neuropathic pain through a prolonged physiochemical stimulation of the acupoint.

The activation of microglia in the dorsal horn of the spinal cord and its surface P2X4R expression after the peripheral nerve injury have a clear effect on the maintenance of nociception^{8,41}. Blocking the P2X4R expression in microglia might be a novel strategy for the treatment of neuropathic pain⁴². The p38MAPK is widely present in neuronal cells and microglia and can exchange information among the pathways. It is involved in the formation and maintenance of neuropathic pain. Studies have shown that, after the sciatic nerve injury, the P2X4R expression on the surface of microglia is upregulated, resulting in the activation and enhanced expression of p-p38MAPK in the neuronal cells; the activation of p-p38 MAPK expression can increase the excitability of neurons and enhance pain perception⁴³. In the current study, Western blot and quantitative real-time PCR analyses suggested that the effects of CS/GP/Fe₃O₄ were better than those of the CS/GP hydrogel in improving the sciatica rats by reducing the expression levels of P2X4R and p38MAPK proteins. This might be related to the responsiveness (stress in the presence of a magnetic field) of the magnetic hydrogel for the acupoints. The effects of CS/GP/Fe₃O₄/DXM hydrogel were better than catgut in improving the analgesic effects on neuropathic pain by decreasing the expression levels of P2X4R and p-p38 MAPK proteins and ensuring a sustained release of DXM. These results showed that the CS/GP hydrogels loaded with drugs could be used as an embedding material for the prolonged stimulation of acupoints.

Altogether, this study showed that the DXM/Fe₃O₄-loaded CS/GP hydrogel had additional advantages in the physiochemical stimulation therapy of acupoint in the CCI

rats. The CS/GP hydrogels loaded with suitable therapeutic drugs might be considered an embedding material similar to the ACET for the physiochemical stimulation of acupoints for the treatment of neuropathic pain. Further *in-vivo* studies on the effects of the magnetic force on acupoints are needed to clarify the clinical applications of this therapy.

Author Contributions

WW collected data and wrote the manuscript. YQH and HJ analyzed data. YY helped to draft the manuscript. YHY made the final modifications. All authors agreed to be accountable for all aspects of the work. All authors read and approved the final manuscript.

Ethical Approval

All the animal experiments in this study were approved by the Laboratory Animal Welfare and Ethics Committee of Shanghai University of Traditional Chinese Medicine (Approval number: PZSHUTCM210115015).

Statement of Human and Animal Rights

The study was performed in strict accordance with the relevant guidelines and regulations.

Statement of Informed Consent

There are no subject in this article and informed consent is not applicable.

Declaration of Conflicting Interests

The author(s) declared no potential conflicts of interest with respect to the research, authorship, and/or publication of this article.

Funding

The author(s) disclosed receipt of the following financial support for the research, authorship, and/or publication of this article: This study was funded by a grant from the National Natural Science Foundation of China (No. 81473759).

ORCID iD

Huayuan Yang  <https://orcid.org/0000-0002-6984-6704>

References

1. Langevin HM, Yandow JA. Relationship of acupuncture points and meridians to connective tissue planes. *Anat Rec.* 2002; 269(6):257–65.
2. Feng Y, Fang Y, Wang Y, Hao Y. Acupoint therapy on diabetes mellitus and its common chronic complications: a review of its mechanisms. *Biomed Res Int.* 2018;2018:3128378–79.
3. Zhang YR, Zhang YJ, Chen X, Xu K, Huang MY, Tan SC, Zhou ZY. Acupoint catgut embedding for the treatment of sciatica: a protocol for a systematic review. *Medicine.* 2021;100(1):e23951.
4. Wen J, Chen X, Yang Y, Liu J, Li E, Liu J, Zhou Z, Wu W, He K. Acupuncture medical therapy and its underlying mechanisms: a systematic review. *Am J Chinese Med.* 2020; 49(01):21–23.

5. Luo D, Liu L, Huang Q, Zhang HM, Chen R. Crosstalk between acupuncture and NF- κ B in inflammatory diseases. *Evid-based Compl Alt*. 2020;24:1–7.
6. Ahmed M. Dexamethasone versus magnesium sulfate as an adjuvant to local anesthetics in the ultra-sound guided injection of piriformis muscle for the treatment of piriformis syndrome. *Open Anesthesiol J*. 2020;14(1):35–41.
7. Radnovich R, Heinz J, Ambrose C, Stannard E, Lissin D. Repeat epidural injections of SP-102 (dexamethasone sodium phosphate injectable gel) in subjects with lumbosacral radiculopathy. *J Pain Res*. 2021;14:1231–39.
8. Stokes L, Layhadi JA, Bibic L, Dhuna K, Fountain SJ. P2X4 receptor function in the nervous system and current breakthroughs in pharmacology. *Front Pharmacol*. 2017;8:291.
9. Trang T, Salter MW. P2X4 purinoceptor signaling in chronic pain. *Purinerg Sig*. 2012;8(3):621–28.
10. He YN. A review of PGLA model of medical materials in clinical catgut embedding application. *Adv Mat Res*. 2015;1096:224–27.
11. Fu S, Zhang P. Design and optimization of a novel chitosan coating system for acupoint catgut embedding materials. *Text Res J*. 2019;89(8):1557–72.
12. Maharjan B, Park J, Kaliannagounder VK, Awasthi GP, Kim CS. Regenerated cellulose nanofiber reinforced chitosan hydrogel scaffolds for bone tissue engineering. *Carbohydr Polym*. 2020;251:117023.
13. Réthoré G, Boyer C, Kouadio K, Toure A, Weiss P. Silanization of chitosan and hydrogel preparation for skeletal tissue engineering. *Polymers*. 2020;12(12):E2823.
14. Mmi A, Lmt B, Lm A. New formulations based on salicylimine-chitosan hydrogels for prolonged drug release. *Int J Biol Macromol*. 2020;160:398–408.
15. Lou C, Tian X, Deng H, Wang Y, Jiang X. Dialdehyde — cyclodextrin-crosslinked carboxymethyl chitosan hydrogel for drug release. *Carbohydr Polym*. 2020;231:115678.
16. Chutatape A, Menon M, Fook-Chong S, George JM. Metabolic and endocrinal effects of epidural glucocorticoid injections. *Singapore Med J*. 2019;60(3):140–44.
17. Sudarsan S, Selvi MS, Chitra G, Sakthivel M, Guhanathan S. Nontoxic pH-sensitive silver nanocomposite hydrogels for potential wound healing applications. *Polym-Plast Tech Mat*. 2020;60(1):84–104.
18. Bayat MR, Baghani M. A review on swelling theories of pH-sensitive hydrogels. *J Intel Mat Syst Str*. 2021;32:18–19.
19. Lee JS, Nah H, Moon HJ, Sang JL, Kwon IK. Controllable delivery system: a temperature and pH-responsive injectable hydrogel from succinylated chitosan. *Appl Surf Sci*. 2020;528:146812.
20. Hoang Thi TT, Sinh LH, Huynh DP, Nguyen DH, Huynh C. Self-assemblable polymer smart-blocks for temperature-induced injectable hydrogel in biomedical applications. *Front Chem*. 2020;8:19.
21. Lavanya K, Chandran SV, Balagangadharan K, Selvamurugan N. Temperature- and pH-responsive chitosan-based injectable hydrogels for bone tissue engineering. *Mater Sci Eng C Mater Biol Appl*. 2020;111:110862.
22. Qian KY, Song Y, Yan X, Dong L, Xue J, Xu Y, Wang B, Cao B, Hou Q, Peng W, Hu J, et al. Injectable ferrimagnetic silk fibroin hydrogel for magnetic hyperthermia ablation of deep tumor. *Biomaterials*. 2020;259:120299–99.
23. Sandra AC, Manuel GF, Ana RT, Mendes BB, Pedro SB, Suzanne MM, Suzanne MM, Anthony W, Rui MA, Domingues R, Reis RL, et al. Injectable and magnetic responsive hydrogels with bioinspired ordered structures. *ACS Biomater Sci Eng*. 2019;5(3):1392–1404.
24. Wang Y, Li B, Xu F, Han Z, Wei D, Jia D, Zhou Y. Tough magnetic chitosan hydrogel nanocomposites for remotely stimulated drug release. *Biomacromolecules*. 2018;19(8):3351–60.
25. Tang J, Qiao Y, Chu Y, Tong Z, Zhou Y, Zhang W, Xie S, Hu J, Wang T. Magnetic double-network hydrogels for tissue hyperthermia and drug release. *J Mater Chem B*. 2019(8):1311–21.
26. Rashidzadeh B, Shokri E, Mahdavinia GR, Moradi R, Abdi S. Preparation and characterization of antibacterial magnetic/pH-sensitive alginate/Ag/Fe₃O₄ hydrogel beads for controlled drug release. *Int J Biol Macromol*. 2020;154(9):134–41.
27. Fu SJ, Zhang PH. Surface modification of polylactic acid and poly (D, L-lactide-co-glycolide) biodegradable materials via chitosan-coating treatment: a new approach for developing novel antibacterial acupoint catgut embedding materials. *Text Res J*. 2019;89(13):2583–94.
28. Kot BCW, Zhang ZJ, Lee AWC, Leung VYF, Fu SN. Elastic modulus of muscle and tendon with shear wave ultrasound elastography: variations with different technical settings. *PLoS ONE*. 2012;7(8):e44348–48.
29. Chung YM, Simmons KL, Gutowska A, Jeong B. Sol-gel transition temperature of PLGA-g-PEG aqueous solutions. *Biomacromolecules*. 2002;3(3):511–16.
30. Dijkstra IM, de Haas AH, Brouwer N, Boddeke HW, Biber K. Challenge with innate and protein antigens induces CCR7 expression by microglia in vitro and in vivo. *Glia*. 2006;54(8):861–72.
31. Cheng YH, Tsai TH, Jhan YY, Chiu WH, Tsai KL, Chien CS, Chiou SH, Liu JL. Thermosensitive chitosan-based hydrogel as a topical ocular drug delivery system of latanoprost for glaucoma treatment. *Carbohydr Polym*. 2016;144:390–99.
32. Xu X, Gu Z, Chen X, Shi C, Liu C, Liu M, Wang L, Sun M, Zhang K, Liu Q. An injectable and thermosensitive hydrogel: promoting periodontal regeneration by controlled-release of aspirin and erythropoietin. *Acta Biomater*. 2019;86:235–46.
33. Kim OG, Kim N, Kim DY, Kwon JS, Min HB. An electrostatically crosslinked chitosan hydrogel as a drug carrier. *Molecules*. 2012;17:13704–11.
34. Zhou HY, Chen XG, Kong M, Liu CS, Cha DS, Kennedy JF. Effect of molecular weight and degree of chitosan deacetylation on the preparation and characteristics of chitosan thermosensitive hydrogel as a delivery system. *Carbohydr Polym*. 2007;73(2):265–73.
35. Das D, Ghosh P, Dhara S, Panda AB, Pal S. Dextrin and poly(acrylic acid)-based biodegradable, non-cytotoxic, chemically cross-linked hydrogel for sustained release of ornidazole and ciprofloxacin. *ACS Appl Mater Interfaces*. 2015;7(8):4791–4803.
36. Guneli E, Onal A, Ates M, Bagriyanik HA, Gumustekin M. Effects of repeated administered ghrelin on chronic constriction injury of the sciatic nerve in rats. *Neurosci Lett*. 2010;479(8):226–30.
37. Zhao XY, Zhang QS, Yang J, Sun FJ, Wang DX, Wang CH, He WY. The role of arginine vasopressin in electroacupuncture treatment of primary sciatica in human. *Neuropeptides*. 2015;52:61–65.
38. Zhao WS, Jiang ZN, Shi H, Xu LL, Yang Y, Wang YC. Low-frequency electroacupuncture alleviates chronic constrictive

- injury-induced mechanical allodynia by inhibiting NR2B upregulation in ipsilateral spinal dorsal horn in rats. *Chin J Integr Med.* 2019;25(6):462–67.
39. Xu Q, Tao L, Chen S, Gao Y, Wang J, Qiao L, Liu J. Correlation between the cumulative analgesic effect of electroacupuncture intervention and synaptic plasticity of hypothalamic paraventricular nucleus neurons in rats with sciatica. *Neural Regen Res.* 2013;8(3):218–25.
40. Liu ZH, Miao GS, Wang JN, Yang CX, Fu ZJ, Sun T. Resolvin D1 inhibits mechanical hypersensitivity in sciatica by modulating the expression of nuclear factor- κ B, phospho-extracellular signal-regulated kinase, and pro- and antiinflammatory cytokines in the spinal cord and dorsal root ganglion. *Anesthesiology.* 2016;124(4):934–44.
41. Trang T, Beggs S, Salter MW. ATP receptors gate microglia signaling in neuropathic pain. *Exp Neurol.* 2012;234(2):354–61.
42. Chen XM, Xu J, Song JG, Zheng BJ, Wang XR. Electroacupuncture inhibits excessive interferon-gamma evoked up-regulation of P2X4 receptor in spinal microglia in a CCI rat model for neuropathic pain. *Br J Anaesth.* 2015;114(1):150–57.
43. Zhou TT, Chen ZY, Wu JR, Liu ZX, Miao B. Effects of dexmedetomidine on P2X4Rs, p38-MAPK and BDNF in spinal microglia in rats with spared nerve injury. *Behav Brain Res.* 2014;1568:21–30.